Understanding Endothelial Glycocalyx Function Under Flow Shear Stress from a Molecular Perspective

Xi Zhuo Jiang[1], Yufang Lu[2], Kai H. Luo[1]*, Yiannis Ventikos[1]*

1. Department of Mechanical Engineering, University College London, Torrington Place, London, UK

2. Department of Automotive Engineering, Tsinghua University, Beijing, P.R. China

*****Corresponding Authors:

Emails: k.luo@ucl.ac.uk (Kai H. Luo); y.ventikos@ucl.ac.uk (Yiannis Ventikos)

Postal Address: Department of Mechanical Engineering, University College London, Torrington Place, London WC1E 7JE, UK

Short title:

Understand EG function from molecular dynamics

Keywords:

molecular dynamics, mechanotransduction, redistribution, pathway, deformation

Abstract

BACKGROUND:

The endothelial glycocalyx plays a pivotal role in regulating blood flow, filtering blood components, sensing and transducing mechanical signals. These functions are intimately related to its dynamics at the molecular level.

OBJECTIVE:

The objective of this research is to establish the relationship between the functions of the endothelial glycocalyx and its dynamics at the molecular level.

METHODS:

To establish such a relationship, large-scale molecular dynamics simulations were undertaken to mimic the dynamics of the glycocalyx and its components in the presence of flow shear stresses.

RESULTS:

First, motions of the glycocalyx core protein and the pertinent subdomains were scrutinised. Three-directional movements of the glycocalyx core protein were observed, although the flow was imposed only in the *x* direction. Such an observation contributes to understanding the glycocalyx redistribution as reported in experiments. Unsynchronised motion of the core protein subdomains was also spotted, which provides an alternative explanation of macroscopic phenomena. Moreover, the dynamics, root-mean-square-deviations and conformational changes of the sugar chains were investigated. Based on the findings, an alternative force transmission pathway, the role of sugar chains, and potential influence on signalling transduction pathway were proposed and discussed.

CONCLUSIONS:

This study relates the functions of the glycocalyx with its microscopic dynamics, which fills a knowledge gap about the links between different scales.

1. Introduction

The glycocalyx, which is an integral part of the vascular barrier, covers all healthy vascular endothelium. It has been confirmed that in patients with cardiovascular risk factors, such as diabetes and hypertension, endothelial glycocalyx damage drives progression of kidney disease and cardiovascular disease (1). The glycocalyx is a complex layer of membrane-bound proteoglycans (e.g. syndecans or glypicans), glycoproteins and glycolipids. A Proteoglycan element consists of a core protein that carries one or more covalently attached glycosaminoglycan (GAG) chains. The main GAGs found on proteoglycans in the endothelial surface layer are heparan sulfate (HS), chondroitin sulfate and dermatan sulfate (2) featuring the highly negative charges (3). It is widely believed that the negatively charged GAGs in the endothelial glycocalyx capture circulating plasma protein and form an interconnected gel-like structure in an aqueous environment (4). The gel-like structure lines the luminal endothelial surface and acts as a barrier against albumin filtration, which is crucial in maintaining the normal function of the glycocalyx (5).

The endothelial glycocalyx is exposed to the mechanical forces of blood flow. Thus, another function of the glycocalyx is a medium for mechanotransduction. Mechanotransduction means the glycocalyx senses the shear stress of flowing blood and transmits the mechanical signal into the cytoplasm (6, 7). The primary evidence that supports a major role for the endothelial glycocalyx layer in mechanotransduction comes from the enzyme degradation experiments. By removing specific components of the glycocalyx, any loss of the glycocalyx functional can be recognised, and the role of the removed part is assessed (2, 8). However, as reviewed in Ref. (9), the drawback of the enzyme degradation method is that it may cause biased estimation of the contribution from the component. Meanwhile, the highly dynamic and fragile sugar chains aggravate the difficulty in *ex vivo* experiments (10).

The functions of the endothelial glycocalyx reported in experiments are intimately related to its dynamics at the molecular scale. However, due to a lack of studies focusing on the dynamics of the glycocalyx, how to establish such a relationship is still unclear. To fill the knowledge gap, we use large-scale molecular dynamics (MD) simulations to mimic the dynamics of the glycocalyx and its components in the presence of flow shear stresses. By discussing the results in the context of experimental studies, functions of the glycocalyx are explained from the perspective of the molecular motions.

2. Methods

2.1 System construction

The up-to-date structure of glycocalyx with the finest resolution (11) has been used to construct the flow/glycocalyx system. As the majority (50% ~ 90% (12)) of GAG chains added to the core proteins of syndecans are of the HS type (13) and for the sake of simplification, only HS sugar chains are considered in the construction of the system. In the proposed system, one glycocalyx element is modelled by the combination of Syndecan-4 (Syn-4) proteoglycan and HS sugar chains. The glycocalyx element can be separated into three parts in accordance with the positions to the lipid membrane: Syn-4 ectodomain connected with sugar chains; Syn-4 transmembrane dimer with a diameter of about 45 Å implanted into a lipid bilayer; and cytoplasmic part of the Syn-4 dimer. The HS length is assumed to be 100 sugar residues (with 4 sugar residues as a linker to Syn-4). Apart from the 4 linker sugar residues, there are 48 disaccharide units for each chain. The end-to-end distance of the HS sugar chains varies from 23 to 41 nm. The HS sugar chains are covalently attached to three serine residues in the Syn-4 ectodomain. The disaccharide sequences of HS sugar chains are introduced in detail in Ref. (11). As reported in Ref. (11), the mean value for bending stiffness of HS sugar chains is 68 $pN{\cdot}nm^2$, which is approximately an order-of-magnitude lower than the value commonly used in continuum glycocalyx

models (490 $pN \cdot nm^2$). As a real endothelial surface environment is far more complicated and heterogenous than the system we proposed in this research, the high value for glycocalyx cannot be attributed to the HS chains alone. All the other macromolecules (e.g. plasma proteins) which are not considered in this research can contribute to the high values for bending stiffness of the glycocalyx. Most of the HS sugar chains in the proposed system are set perpendicular (or nearly perpendicular) to the endothelial cell surface, which corresponds to the newly published observation from Stochastic Optical Reconstruction Microscopy (14). The Syn-4 intracellular domain is not linked to the cytoskeleton.

Figure 1a illustrates an overview of the flow/glycocalyx system with its initial configuration. The lipid bilayer separates the simulation domain into two regions. Ectodomain, where blood flows in the lumen, is over the lipid bilayer. The ectodomain is filled with the ectodomain part of the Syn-4 core protein, HS sugar chains connected to the protein, ions and water molecules. The cytoplasm, namely the inner domain of the cell, is below the lipid bilayer. The cytoplasmic part of the Syn-4 protein, ions and water molecules are the main components of this region. The glycocalyx features its negative charge and the charge distribution depends on the geometry distributions of the sugar chains. A NaCl aqueous solution with a concentration of 0.1 M was used to neutralize and solvate the biomolecules. According to our previous study (15), these charges (the negative sugar chains, Na^+ and Cl^-) are not uniformly distributed along the space in the ectodomain. The spatial distributions of the charges can be referred to Ref. (15). For the three directions (i.e. *x*-, *y*- and *z*-directions), periodic boundary conditions were applied. Details about the set-up for the boundary conditions can be found in previous publications (16-18).

In the flow/glycocalyx model, three glycocalyx elements are constructed and implanted on the lipid bilayer. Each glycocalyx element (i.e. proteoglycan) bears six HS chains glued to the ectodomain of the Syn-4 core protein dimer. The blood flow is simulated by driving the ectodomain water molecules via

external forces on water oxygens. The dimension of the domain simulated is a hexagonal area of 820 nm^2 by 72 nm in height. About 5,800,000 atoms are contained in the entire flow/glycocalyx system (18).

2.2 Protocol details

The TIP3P water model (19) was adopted to simulate water molecules. A CHARMM biomolecular force field (20) was applied on the proteins and the lipid bilayer.

An equilibrium simulation was first conducted at 1 atm and 310K (NPT ensemble), using a Langevin thermostat and a Nosé-Hoover Langevin piston for 2 ns, followed by another simulation using a Langevin thermostat to maintain temperature at 310K for 0.5 ns (NVT ensemble). The last frame of the NVT simulation was then used as the initial configuration (as shown in Figure 1a) of the follow-up "production" flow simulations. In the flow simulations, the Lowe-Andersen thermostat was selected to maintain the temperature at 310K.

The velocity Verlet integration method (21) was used to advance the positions and velocities of the atoms in time. A 2-fs timestep, and particle mesh Ewald (22) electrostatics with a grid density of $1/Å^3$ are used. The SETTLE algorithm (23) was used to enable the rigid bonds connected to all hydrogen atoms. The van der Waals interactions were calculated using a cutoff of 12 Å with a switching function starting at 10 Å.

All MD simulations were performed using the software NAMD 2.9 (24). The visualisation of the molecular structures was performed by the VMD (25) package. Post-processing of the MD results was accomplished using PYTHON (Python Software Foundation, Wilmington, De) scripts. All parallel simulations and non-visualised post-processing were conducted on ARCHER, UK's national supercomputing service. To obtain a simulation result with a physical period of 1 ns, 9,000 compute cores have been simultaneously employed for about 2 hours.

2.3 Flow simulation and case set-up

In this research, NaCl solution was used as a simplification of the blood flow. To mimic flow, external forces in the *x* direction were imposed on oxygen atoms of water molecules in the ectodomain, and the tactic was successfully practiced in previous studies (16, 18, 26). In one of our previous studies (18), we reported that an external force of 0.003 fN would generate a laminar flow with a physiological bulk flow velocity (The order of magnitude of the bulk flow velocity is assumed 0.1~1 cm/s, which corresponds to that expected in the human microcirculation.); the presence of the glycocalyx disturbs the flow profiles, resulting in an oscillating velocity distribution in space. To study the dynamics of the endothelial glycocalyx in various situations, four scenarios were established as listed in Table 1. Case I is for mimicking a physiological flow under the intact EG situations with 18 sugar chains. In Case II, the external force is set to 0 to simulate a stationary state. Cases III and IV are two scenarios with shedding of sugar chains by removing of 3 and 9 sugar chains, respectively. The strategy for removal of sugar chains is illustrated in Figures 1b to 1d. Detailed information about the removal strategy was introduced in Ref. (17).

3. Results

3.1 Dynamics of core protein

The trajectory of the core protein of the central glycocalyx element (Figure 2a) is tracked in the case with intact glycocalyx configuration and physiological flow (i.e. Case I). Figure 2b shows the trajectory of the core protein. The curve in Figure 2b represents the trace of the protein in the XOY plane. The circles represent the relative *z* positions of the core protein compared to that at the start point; the area of a circle means the deviation of core protein from its original position in the *z* direction, with the blue colour being higher than the position at the start point and red lower than the start point. As illustrated in the Figure 2b, the core protein travels in the same direction as the flow, as expected. Meanwhile, it also moves in the Y and Z directions.

3.2 Dynamics of core protein subdomains

The motions of the central glycocalyx core protein subdomains are further examined for Case I. The core protein is a Syn-4 dimer, comprising the ectodomain and transmembrane parts with the secondary structures illustrated in Figure 3a. Secondary structures (Figure 3a) show that flexible linkages between subdomains of ectodomain Syn-4 (EA1 and EA2 from Chain A, and EB1 and EB2 from Chain B) as well as Syn-4 ectodomain and transmembrane parts (TA1 and EA1 for Chain A, and TB1 and EB1 for Chain B) encourage the glycocalyx to perform like a soft matter. To study the dynamics of the soft matter, Four distances (d_{A1}, d_{A2}, d_{B1} and d_{B2}) are employed to record positions of the ectodomain and transmembrane Syn-4. As shown in Figure 3b, the first 10 ns witnesses different trends of the four distances. After 10 ns, the average distances with standard errors for the four distances are calculated. The differences in the distance variations further validate the model of the glycocalyx as a soft matter.

3.3 Dynamics of sugar chains

The dynamic and fragile feature of the glycocalyx sugar chains increases the difficulty in glycocalyx-related experiments (9, 10). To gain additional insight into the dynamics of the sugar chain, four segments from two typical sugar chains, labelled P1 to P4 in Figure 4a, are selected for motion inspection. Segments P1 and P3, individually composed of five residues, are located at 40% of the total length of chains 1 and 2, respectively. Segment P2 and segment P4 each comprise the five ending residues of sugar chain tails. Their motions in three directions are recorded as shown in Figures 4b and 4c. In Figure 4b, the *z* positions of these segments indicate that the four segments swing up and down as flow passes by. Figure 4c records the trajectories of the four segments in the XOY plane, and white lines represent their routes during the 30-ns simulation. As illustrated in Figure 4c, these segments also swirl freely in space (18).

3.4 Root-mean-square deviation (RMSD) of sugar chains

Figure 2a suggests that the dynamic sugar chains may interfere with each other. To study how they impede each other, the RMSDs of three sugar chains, as an alternative measure of sugar chain movements, are investigated under situations with varying numbers of sugar chains (i.e. Cases I, III and IV in Table 1). The values of RMSDs are calculated by a build-in plugin of the VMD package (25). Figure 5a highlights the three mutual sugar chains. Their RMSDs under situations with changing sugar chain numbers are summarised in Figure 5b. As the statistics suggest, the RMSD values increase as the number of sugar chain decreases, which implies their interference with each other.

3.5 Conformations of sugar chains

The sugar chains are flexible and dynamic even in the stationary situations. In the stationary case (Case II in Table 1), to describe the dynamics of sugar chains the conformations of two sugar chains, i.e. sugar chains AS and BS in Figure 6a, are investigated. The conformation of a sugar chain is measured via a centre-to-centre vector connecting the two centres of mass of a bisected sugar chain, which is reported effective in describing polymer rotational dynamics (27). The distributions (counted by the occurrence in the recorded frames) for magnitudes, r, of centre-to-centre vectors for the two sugar chains are summarised in Figure 6b. Due to the corner structure, sugar chain BS has a shorter centre-to-centre distance than its stretching counterpart, sugar chains AS.

As illustrated in Figure 6a, the major initial conformational difference of the two sugar chains resides in segments with corner shapes. The sugar chains attract Na^+ ions due to their highly negative charges. To reveal how the corner shape affects the interaction between Na^+ and sugar chains, two segments with identical residue sequence but one featuring a corner shape and the other with a stretching shape are selected. The numbers of Na^+ around both segments (highlighted purple in Figure 6a) throughout the no-flow simulation are recorded. To further explore how the corner conformation influences their

interaction with Na^+ ions, the residence rates of initial Na^+ ions around the corner and stretching conformations are calculated. The residence rate is calculated as

$$\text{residence rate} = \frac{n_{Na,j}}{n_{Na,0}} \quad (1)$$

In Eq. (1), $n_{Na,j}$ is the number of Na^+ ions retained from the initial frame of the simulation at the instant j, and $n_{Na,0}$ is the number of Na^+ ions at the initial frame of the simulation. The distributions (counted by the occurrence in the recorded frames) for the residence rates of both sugar chains are summarised, as shown in Figure 6c., The higher residence rate of Na^+ of sugar chain BS indicates that more ions stay around the corner sugar chain. In other words, the corner conformation accumulates Na^+ by confining the ions within its "realm". By contrast, the stretching structure of sugar chain AS facilitates the motion of ions.

4. Discussion

In this section, the biological significance of the dynamics of the glycocalyx is discussed.

4.1 Glycocalyx redistribution

When exposed to the flow shear stress, the glycocalyx is redistributed as witnessed in experiments (28, 29). For example, the percentage area of the cell membrane coated by the glycocalyx increases after the cells being exposed to the flow shear stress for a certain period (29). It is noteworthy that the simulation time scale is far smaller than its experiment counterpart. However, it is still worthwhile to relate the MD findings with experimental observations, as MD results can capture fine and basic movements of atoms and molecules, which could complement experimental observations. According to our results (Figure 2b), the glycocalyx core protein not only travels along the flow direction but also moves actively in the other two directions. As sugar chains are anchored to the core protein, the flexible movement of the core protein consequently results in varying overlap areas between the sugar chains,

which explains the changes in the percentage area of the cell membrane covered by the glycocalyx as reported in Ref. (29). Although the cytoskeleton is not included in the present simulation, a disturbance in the well-structured cytoskeleton can still be inferred from the dynamic movement of the core protein. The structure disturbance could then cause the reorganisation of the cytoskeleton, thereby resulting in the cell migration along the direction of flow, as reported in previous studies (30, 31).

4.2 Deformation of core protein from an atomic perspective

Molecular dynamics methods provide a unique perspective to understand some macroscopic matrix in continuum studies. For example, in a previous continuum study (32), the authors discussed the bending rigidity of the core proteins that enables them to resist the deformation by fluid shear stresses. If an object is a rigid body, any two points of the body will move simultaneously. Yet, according to our results in Figure 3b, the subdomains of the core protein move unsynchronised. The presumed deformation is indeed the unsynchronisation of the subdomains, with the bending rigidity being a measure of the pertinent synchronization (18).

4.3 Mechanotransduction pathways

Based on the dynamics of the subdomain of the core protein (mentioned in 3.2) and the sugar chains (mentioned in 3.3), the potential mechanotransduction pathway of the glycocalyx can be proposed. One topic about the mechanotransduction of the glycocalyx is to sort out the route via which the flow shear stress is transmitted into the cytoplasm. Previous studies (32, 33) favour that the flow shear stress is first transmitted to the sugar chains and then transmitted to the cytoplasm via the core protein. In our research, the results in Sections 3.2 and 3.3 suggest that the movements of the core protein and the sugar chains are not strongly correlated (with the Pearson correlation coefficients between the z-direction movements of the selected sugar chain segment P1 and Syn-4 ectodomain being -0.35, P2 and Syn-4 ectodomain 0.35, P3 and Syn-4 ectodomain 0.55, and P4 and Syn-4 ectodomain 0.53), which implies that the force

may be transmitted to the cytoplasm via the core protein without the transduction of the sugar chains. These two routes are both potential force transmission pathways via the glycocalyx.

4.4 Function of sugar chains

Figure 5 suggests that the sugar chains interfere with each other, as the RMSD values increase with the reducing number of the sugar chains. Given that the sugar chains are connected to the core protein, albeit weakly correlated, the fierce movement in the sugar chain reduced situations suggests a dynamic movement of the core protein, thereby influencing the mechanotransduction. Therefore, one function of the sugar chains is to prevent the severe movement of the core protein and to maintain the normal function of glycocalyx.

4.5 Implications for initiating signal transduction pathways

As discussed in Ref. (34), blood flow can uncoil the glycocalyx in the direction of flow and the corresponding conformational change can increase Na^+ ion binding sites that initiate signal transduction pathways. In our research, the number of Na^+ ion binding sites was not determined; however, Figure 6 can still demonstrate the importance of the glycocalyx in activating signalling transduction pathways. The conformational difference leads to the variations in the residence rate of Na^+ ions. Combined with the results of sugar chain dynamics (Section 3.3), it is rational to expect an activation of signal channels sensed by the glycocalyx when blood flow velocity changes.

5. Conclusions

In this research, large-scale molecular dynamics simulations were conducted to investigate the dynamics of the glycocalyx on a small patch of the lipid membrane. The motions of the glycocalyx core protein and the pertinent subdomains were scrutinised. Movements of the core protein were observed in all three directions, although the flow was imposed only in the *x* direction. Such a finding contributes to understanding the glycocalyx redistribution as reported in experiments. Unsynchronised motion of the

core protein subdomains provides an alternative explanation of deformation from the molecular perspective. Moreover, the dynamics, RMSDs and conformational changes of the sugar chains were investigated. Based on these findings, an alternative force transmission pathway, the role of sugar chains, and potential influence on signalling transduction pathway have been proposed and discussed. The force from the flow shear stresses can be probably transmitted from the blood flow via the core protein and then to the cytoplasm without going to the sugar chains. One function of the sugar chains is to prevent the severe movement of the core protein and to maintain the normal function of glycocalyx. The changes in blood flow velocities may activate the signalling channels via the pertinent conformational changes of sugar chains.

This study relates the macroscopic behaviour and functions of the glycocalyx with its molecular dynamics, which contributes to filling the knowledge gaps about the links between different scales. Future molecular dynamics studies can focus on the functionality of the glycocalyx serving as a molecular sieve and on the response of the glycocalyx to changes in physiological conditions.

Acknowledgement

This work was supported by the UK Engineering and Physical Sciences Research Council under the project "UK Consortium on Mesoscale Engineering Sciences (UKCOMES)" (Grant Nos. EP/L00030X/1 and No. EP/R029598/1).

290 **References**

291 [1] Rabelink TJ, de Zeeuw D. The glycocalyx—linking albuminuria with renal and cardiovascular
292 disease. Nat Rev Nephrol. 2015;11:667. doi: 10.1038/nrneph.2015.162

293 [2] Weinbaum S, Tarbell JM, Damiano ER. The structure and function of the endothelial glycocalyx
294 layer. Annu Rev Biomed Eng. 2007;9(1):121-67. doi: 10.1146/ annurev.bioeng. 9.060906.151959

295 [3] Sieve I, Munster-Kuhnel AK, Hilfiker-Kleiner D. Regulation and function of endothelial glycocalyx
296 layer in vascular diseases. Vasc Pharmacol. 2018;100:26-33. doi: 10.1016/j.vph.2017.09.002

297 [4] Fu BM, Tarbell JM. Mechano-sensing and transduction by endothelial surface glycocalyx:
298 composition, structure, and function. WIRES Syst Biol Med. 2013;5(3):381-90. doi:
299 10.1002/wsbm.1211

300 [5] Tarbell JM, Cancel LM. The glycocalyx and its significance in human medicine. J Intern Med.
301 2016;280(1):97-113. doi: 10.1111/joim.12465

302 [6] Tarbell JM, Pahakis M. Mechanotransduction and the glycocalyx. J Intern Med. 2006;259(4):339-
303 50. doi: 10.1111/j.1365-2796.2006.01620.x

304 [7] Jaalouk DE, Lammerding J. Mechanotransduction gone awry. Nat Rev Mol Cell Bio.
305 2009;10(1):63-73. doi: 10.1038/nrm2597

306 [8] Pahakis MY, Kosky JR, Dull RO, Tarbell JM. The role of endothelial glycocalyx components in
307 mechanotransduction of fluid shear stress. Biochem Biophys Res Commun. 2007;355(1):228-33. doi:
308 10.1016/j.bbrc.2007.01.137

309 [9] Tarbell JM, Simon SI, Curry FR. Mechanosensing at the vascular interface. Annu Rev Biomed Eng.
310 2014;16:505-32. doi: 10.1146/annurev-bioeng-071813-104908

311 [10]Dane MJC, Berg BMvd, Lee DH, Boels MGS, Tiemeier GL, Avramut MC, et al. A microscopic
312 view on the renal endothelial glycocalyx. Am J Physiol-Renal Physiol. 2015;308(9):F956-F66. doi:

10.1152/ajprenal.00532.2014

[11] Cruz-Chu ER, Malafeev A, Pajarskas T, Pivkin IV, Koumoutsakos P. Structure and response to flow of the glycocalyx layer. Biophys J. 2014;106(1):232-43. doi: 10.1016/j.bpj.2013.09.060

[12] Reitsma S, Slaaf DW, Vink H, van Zandvoort MAMJ, oude Egbrink MGA. The endothelial glycocalyx: composition, functions, and visualization. Pflüg Arch Eur J Physiol. 2007;454(3):345-59. doi: 10.1007/s00424-007-0212-8

[13] Deepa SS, Yamada S, Zako M, Goldberger O, Sugahara K. Chondroitin sulfate chains on syndecan-1 and syndecan-4 from normal murine mammary gland epithelial cells are structurally and functionally distinct and cooperate with heparan sulfate chains to bind growth factors. A novel function to control binding of midkine, pleiotrophin, and basic fibroblast growth factor. J of biol Chem. 2004;279(36):37368-76. doi: 10.1074/jbc.M403031200

[14] Xia Y, Fu BM. Investigation of endothelial surface glycocalyx components and ultrastructure by single molecule localization microscopy: Stochastic Optical Reconstruction Microscopy (STORM). Yale J Biol Med. 2018;91(3):257-66.

[15] Jiang XZ, Luo KH, Ventikos Y. Reducing Salt Intake and Exercising Regularly: Implications From Molecular Dynamics Simulations of Endothelial Glycocalyx. Front Physiol. 2018;9(1667). doi: 10.3389/fphys.2018.01667

[16] Jiang XZ, Feng M, Luo KH, Ventikos Y. Large-scale molecular dynamics simulation of flow under complex structure of endothelial glycocalyx. Comput Fluids. 2018;173:140-6. doi: 10.1016/j.compfluid.2018.03.014

[17] Jiang XZ, Feng M, Ventikos Y, Luo KH. Regimes of Flow over Complex Structures of Endothelial Glycocalyx: A Molecular Dynamics Simulation Study. Sci Rep. 2018;8(1):5732. doi: 10.1038/s41598-018-24041-7

[18] Jiang XZ, Gong H, Luo KH, Ventikos Y. Large-scale molecular dynamics simulation of coupled dynamics of flow and glycocalyx: towards understanding atomic events on an endothelial cell surface. J R Soc Interface. 2017;14(137). doi: 10.1098/rsif.2017.0780

[19] Jorgensen WL, Chandrasekhar J, Madura JD, Impey RW, Klein ML. Comparison of simple potential functions for simulating liquid water. J Chem Phys. 1983;79(2):926-35. doi: 10.1063/1.445869

[20] MacKerell AD, Bashford D, Bellott M, Dunbrack RL, Evanseck JD, Field MJ, et al. All-atom empirical potential for molecular modeling and dynamics studies of proteins. J Phys Chem B. 1998;102(18):3586-616.

[21] Allen MPA, Tildesley DJ. Computer Simulation of Liquids. New York: Oxford University Press; 1987.

[22] Darden T, York D, Pedersen L. Particle mesh Ewald: An N·log(N) method for Ewald sums in large systems. J Chem Phys. 1993;98(12):10089-92. doi: 10.1063/1.464397

[23] Miyamoto S, Kollman PA. Settle - an analytical version of the Shake and Rattle algorithm for rigid water models. J Comput Chem. 1992;13(8):952-62. doi: 10.1002/jcc.540130805

[24] Phillips JC, Braun R, Wang W, Gumbart J, Tajkhorshid E, Villa E, et al. Scalable molecular dynamics with NAMD. J Computat Chem. 2005;26(16):1781-802. doi: 10.1002/jcc.20289

[25] Humphrey W, Dalke A, Schulten K. VMD: Visual molecular dynamics. J Mol Graph Model. 1996;14(1):33-8. doi: 10.1016/0263-7855(96)00018-5

[26] Pikoula M, Tessier MB, Woods RJ, Ventikos Y. Oligosaccharide model of the vascular endothelial glycocalyx in physiological flow. Microfluid Nanofluidics. 2018;22(2):21. doi: 10.1007/s10404-018-2037-5

[27] Kim JM, Baig C. Precise Analysis of Polymer Rotational Dynamics. Sci Rep. 2016;6:19127. doi: 10.1038/srep19127

[28]Li W, Wang W. Structural alteration of the endothelial glycocalyx: contribution of the actin cytoskeleton. Biomech Model Mechanobiol. 2018;17(1):147-58. doi: 10.1007/s10237-017-0950-2

[29]Bai K, Wang W. Shear stress-induced redistribution of the glycocalyx on endothelial cells in vitro. Biomech Model Mechanobiol. 2014;13(2):303-11. doi: 10.1007/s10237-013-0502-3

[30]Moon JJ, Matsumoto M, Patel S, Lee L, Guan JL, Li S. Role of cell surface heparan sulfate proteoglycans in endothelial cell migration and mechanotransduction. J Cell Physiol. 2005;203(1):166-76. doi: 10.1002/jcp.20220

[31]Ebong EE, Lopez-Quintero SV, Rizzo V, Spray DC, Tarbell JM. Shear-induced endothelial NOS activation and remodeling via heparan sulfate, glypican-1, and syndecan-1. Integrat Biol. 2014;6(3):338-47. doi: 10.1039/c3ib40199e

[32]Weinbaum S, Zhang X, Han Y, Vink H, Cowin SC. Mechanotransduction and flow across the endothelial glycocalyx. Proc Natl Acad Sci U S A. 2003;100(13):7988-95. doi: 10.1073/pnas.1332808100

[33]Thi MM, Tarbell JM, Weinbaum S, Spray DC. The role of the glycocalyx in reorganization of the actin cytoskeleton under fluid shear stress: a "bumper-car" model. Proc Natl Acad Sci U S A. 2004;101(47):16483-8. doi: 10.1073/pnas.0407474101

[34]Johnson BD, Mather KJ, Wallace JP. Mechanotransduction of shear in the endothelium: Basic studies and clinical implications. Vasc Med. 2011;16(5):365-77. doi: 10.1177/1358863X11422109

Table 1 Summary of simulation cases in this study

Case	external force / fN	Number of sugar chains, N	Physical time / ns
I	0.003	18	30
II	0	18	8
III	0.003	15	15
IV	0.003	9	15

382 **Figure legends**

383 **Figure 1 Initial configuration of the all-atom glycocalyx-flow system and the strategy of removing**
384 **sugar chains.** a. Initial configuration. The system includes 3 Syn-4 dimers as proteoglycans, 18 sugar
385 chains attached on the apexes of Syn-4 dimers and a lipid bilayer. External forces are imposed in the *x*
386 direction on the water molecules in the ectodomain. Water molecules and ions are not shown. b. Top
387 view of sugar chain layout in the complete flow/glycocalyx system for Cases I and II in Table 1. c. Top
388 view of a reduced flow/glycocalyx system (Case III in Table 1) with three sugar chains (highlighted red
389 in Panel b) removed from the central glycocalyx element. d. Top view of a reduced flow/glycocalyx
390 system (Case IV in Table 1) with half of sugar chains removed (highlighted sugar chains in Panels b and
391 c). In Panels b, c and d, only sugar chain layouts are illustrated. Details can be found in Ref. (13).

392 **Figure 2 Motion of the central glycocalyx core protein.** a. Top view of the glycocalyx elements with
393 the lipid membrane (Only the glycocalyx elements and the lipid membrane are shown). b. The 30-ns
394 trajectory of the core protein of the central glycocalyx element from case I. The core protein moves in
395 three directions.

396 **Figure 3 Motion of subdomain of central glycocalyx core protein.** a. Central glycocalyx core
397 protein with its secondary structure. b. Four distances used to depict the motions of the subdomains of
398 the central glycocalyx core protein.

399 **Figure 4 Dynamics of four segments from two sugar chains.** a. Four segments from two sugar
400 chains are selected to investigate the dynamics of sugar chains. b. The *z*-direction positions of these four
401 sugar chains as flow passes by. c. The four segments swirl freely in the XOY plane.

402 **Figure 5 The root-mean-square-deviations (RMSDs) of the intact sugar chains of the central**

glycocalyx element. a. The intact sugar chains are highlighted in magenta. b. The RMSDs of the three sugar chains in three sugar-chain shedding scenarios. N=18 (Case I in Table 1) means no shedding sugar chains, N=15 (case III in Table 1) refers to the scenario with the removal of the three sugar chains of the central glycocalyx element, and N=9 (case IV in Table 1) represents the scenario with the removal of half number of the sugar chains. Generally, the surrounding sugar chains impede the movement of the central sugar chains, according to the small variations in the N=18 case. (*$p < 0.05$; **$p < 0.01$; ***$p < 0.001$ by F-test)

Figure 6 Conformations of two sugar chains and residence rate distributions of Na^+ around individual sugar chains. a. Two sugar chains with identical residue sequence but different initial conformations. b. Distributions for centre-to-centre lengths, *r*, of both sugar chains. c. The residence rate distributions of Na^+ ions around the corner segment and its stretching counterpart.

Figure 1

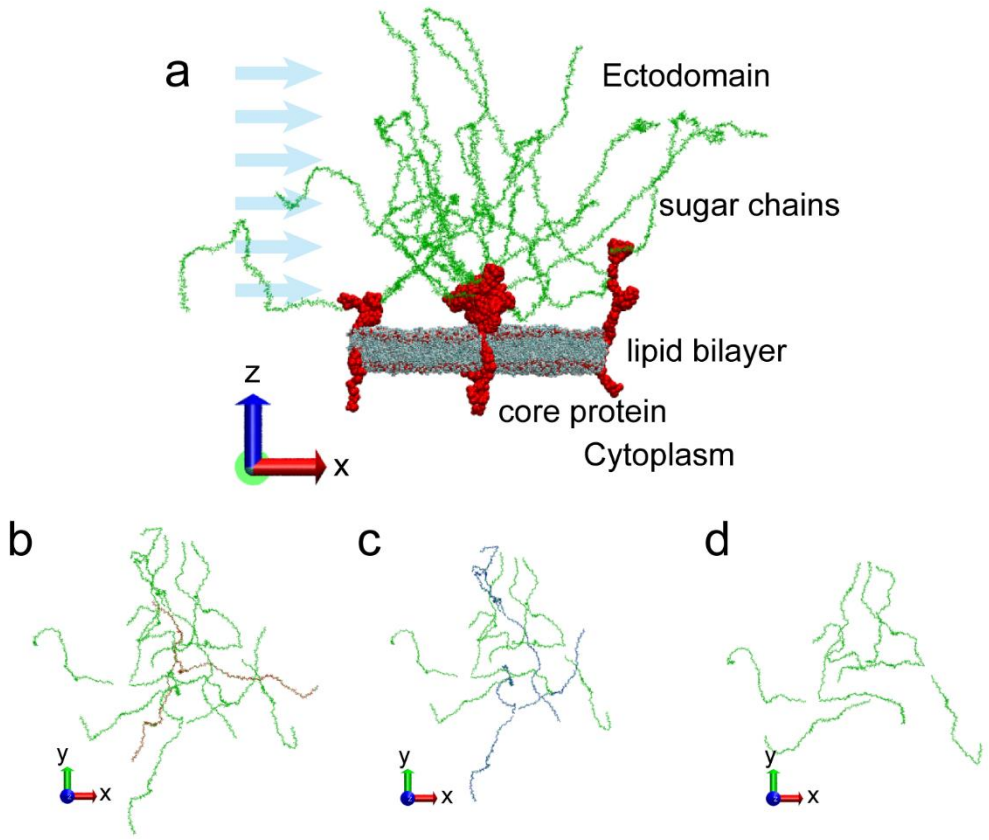
a
Ectodomain
sugar chains
lipid bilayer
core protein
Cytoplasm
z
x
b
y
x
c
y
x
d
y
x

Figure 2

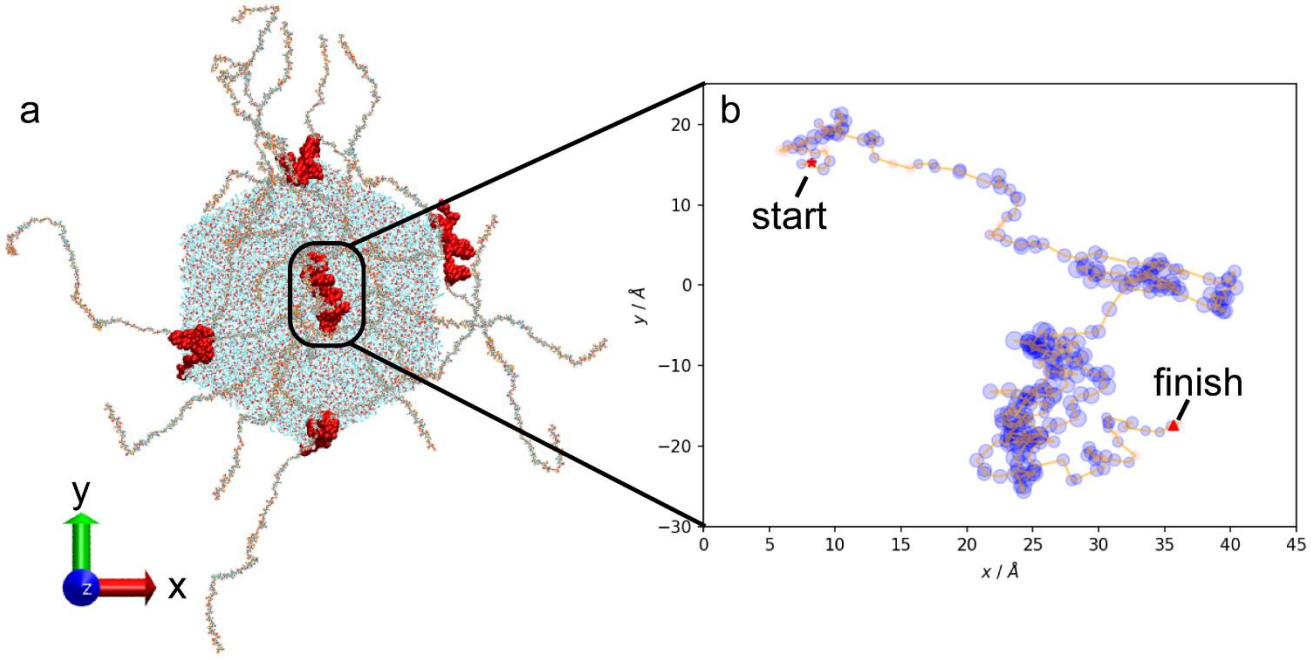

Figure 3

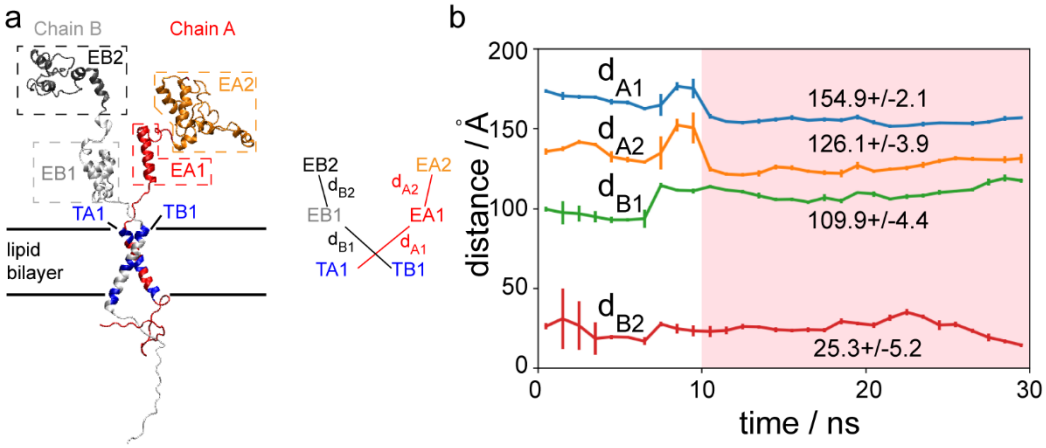
a
Chain B
Chain A
EB2
EA2
EB1
EA1
TA1
TB1
lipid
bilayer
EB2
EA2
EB1
EA1
TA1
TB1
b
distance / Å
time / ns
154.9+/-2.1
126.1+/-3.9
109.9+/-4.4
25.3+/-5.2

425 **Figure 4**

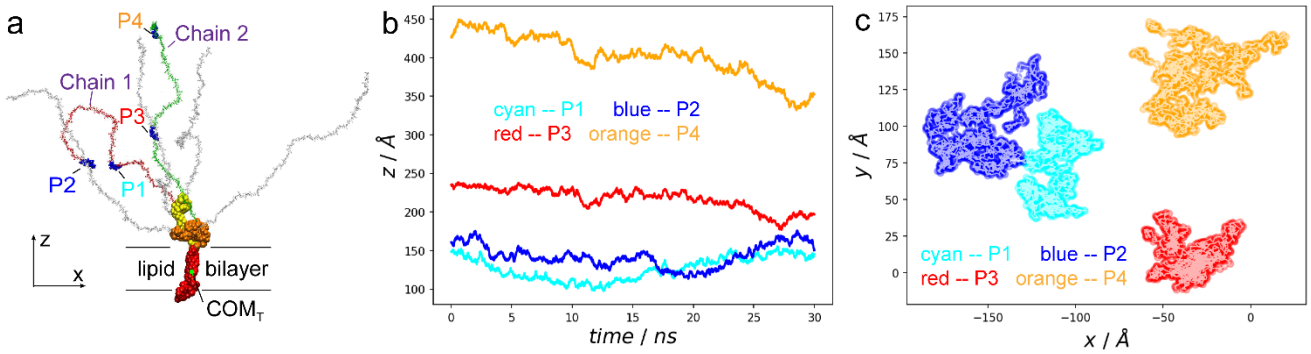

426

427

Figure 5

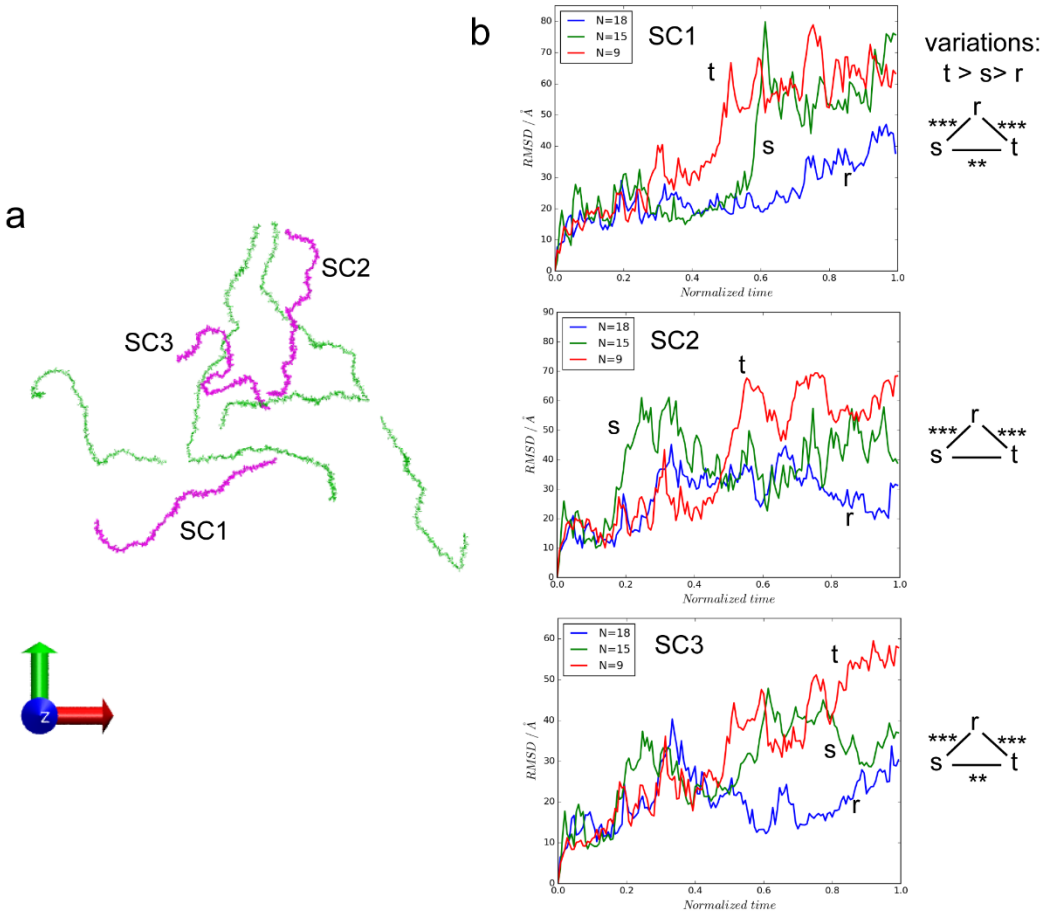
a
SC2
SC3
SC1
Z
b
N=18
N=15
N=9
SC1
t
s
r
RMSD / Å
Normalized time
variations:
t > s> r
***
**
SC2
SC3

Figure 6